Isolating Individual Trees in a Savanna Woodland Using Small Footprint Lidar Data

Qi Chen, Dennis Baldocchi, Peng Gong, and Maggi Kelly

Abstract

This study presents a new method of detecting individual treetops from lidar data and applies marker-controlled watershed segmentation into isolating individual trees in savanna woodland. The treetops were detected by searching local maxima in a canopy maxima model (CMM) with variable window sizes. Different from previous methods, the variable windows sizes were determined by the lower-limit of the prediction intervals of the regression curve between crown size and tree height. The canopy maxima model was created to reduce the commission errors of treetop detection. Treetops were also detected based on the fact that they are typically located around the center of crowns. The tree delineation accuracy was evaluated by a five-fold, cross-validation method. Results showed that the absolute accuracy of tree isolation was 64.1 percent, which was much higher than the accuracy of the method, which only searched local maxima within window sizes determined by the regression curve (37.0 percent).

Introduction

Isolating individual trees and extracting relevant tree structure information from remotely sensed data have significant implications in a variety of applications. For example, detailed information at the individual tree level can be used for monitoring forest regeneration (Gougeon and Leckie, 1999; Clark *et al.*, 2004a and 2004b), reducing fieldwork required for forest inventory (Gong *et al.*, 1999) and assessing forest damage (Leckie *et al.*, 1992; Levesque and King, 1999; Kelly *et al.*, 2004). To study the interactions between vegetation and climate, we are applying an individual tree-based model, called MAESTRA, over an eddy covariance tower site in Ione, California for quantifying the carbon fluxes. To parameterize the individual tree-based model, our research is ongoing to extract individual tree structure parameters such as tree height, crown height, crown size, leaf area index (LAI), and biomass using small-footprint lidar data over an area of 800 m by 800 m around the eddy covariance tower. However, to obtain such individual tree parameters, the initial process is to isolate individual trees and delineate tree crown boundaries.

Intensive research has been done on isolating individual trees using remotely sensed data. However, previous data focuses on large-scale aerial photos or high-spatial resolution remotely sensed imagery. The methods for isolating individual trees from imagery or photos include: local maxima detection (Dralle and Rudemo, 1996), local maxima filtering with fixed or variable window sizes (Wulder *et al.*, 2000; Pouliot *et al.*, 2002), valley-following (Gougeon, 1995), edge detection using scale-space theory (Brandtberg and Walter, 1998), template-matching (Pollock, 1996; Larsen and Rudemo, 1998), local transect analysis (Pouliot *et al.*, 2002), 3D modeling (Sheng *et al.*, 2001; Gong *et al.*, 2002), and watershed segmentation (Schardt *et al.*, 2002; Wang *et al.*, 2004). When isolating trees from a monocular image or photo, these methods are mostly based on the assumption that there are "peaks" of reflectance around the treetops and "valleys" along the canopy edges. However, the "peaks" and "valleys" are not always distinct since canopy reflectance is affected by various factors such as illumination conditions, canopy spectral properties, and complex canopy structure.

Recently, researchers have begun to apply lidar data into individual tree isolation and canopy information extraction (Hyyppä *et al.*, 2001; Persson *et al.*, 2002; Brandtberg *et al.*, 2003; Leckie *et al.*, 2003; Popescu *et al.*, 2003; Popescu and Wynne, 2004). Compared with passive imaging, lidar has the advantage of directly measuring the three-dimensional coordinates of canopies. Therefore, the geometric, rather than spectral, "peaks" and "valleys" can be detected. Several studies have extended methods developed for optical imagery and aerial photos into lidar data for tree detection (Brandtberg *et al.*, 2003; Leckie *et al.*, 2003; Popescu *et al.*, 2003). Brandtberg *et al.* (2003) extended the scale-space theory to detecting crown segments. Leckie *et al.* (2003) applied the valley-following approach into both lidar and multi-spectral imagery and found that the lidar can easily eliminate most of the commission errors that occur in the open stands while the optical imagery performs better for isolating trees in Douglas-fir plots.

This study attempts to use marker-controlled watershed segmentation in tree isolation. Watershed segmentation, first proposed by Beucher and Lantuejoul (1979), is a well-known image segmentation method that incorporates the advantages of other segmentation methods such as region-growing and edge-detection (Soille, 2003). To avoid the over-segmentation problem, Meyer and Beucher (1990) introduced

Qi Chen is with the Center for the Assessment and Monitoring of Forest and Environmental Resources (CAMFER), University of California at Berkeley, Berkeley, CA 94720 (qch@nature.berkeley.edu).

Dennis Baldocchi is with the Department of Environmental Science, Policy, and Management, University of California at Berkeley, Berkeley, CA 94720 (baldocchi@nature.berkeley.edu).

Peng Gong and Maggi Kelly are with the Center for the Assessment and Monitoring of Forest and Environmental Resources (CAMFER), University of California at Berkeley, Berkeley, CA 94720 (gong@nature.berkeley.edu; mkelly@nature.berkeley.edu).

Photogrammetric Engineering & Remote Sensing
Vol. 72, No. 8, August 2006, pp. 923–932.

0099-1112/06/7208–0923/$3.00/0

marker-controlled watershed segmentation. The idea is to perform watershed segmentation around user-specified markers rather than the local maxima in the input image. The image indicating the locations of markers is called a *marker function* and the image for producing watersheds is called a *segmentation function*. Marker-controlled watershed segmentation is well-suited for tree isolation. With appropriate marker and segmentation functions, marker-controlled watershed segmentation can be used to delineate the boundaries of individual crowns. This characteristic makes it superior to local transect or profile methods (Pouliot *et al.*, 2002; Popescu *et al.*, 2003), which can only obtain crown radii for limited directions.

Marker-controlled watershed segmentation was applied for tree isolation in a Compact Airborne Spectrographic Imager (CASI) image (Wang *et al.*, 2004). Schardt *et al.* (2002) used the threshold for isolating spruce trees in lidar data and suspected it to be unsuitable for deciduous tree species due to their complex canopy structure. In marker-controlled watershed segmentation, the forms of marker and segmentation functions play a key role in partitioning an image to meaningful objects. In particular, marker functions corresponding to treetops are crucial for its successful application in tree isolation. This study hypothesizes that individual trees can be isolated for deciduous trees only if appropriate marker and segmentation functions are generated from lidar data. Based on these, the objectives of this study are to present methods for generating treetop marker and segmentation functions from lidar data and test their application into tree isolation in savanna woodland

This paper is organized as follows: first, the methods of treetop detection with variable window sizes are discussed and a new method of creating marker and segmentation functions is introduced; next, the performance of these markers and segmentation functions is evaluated and relevant errors are analyzed; and finally, the conclusions are presented.

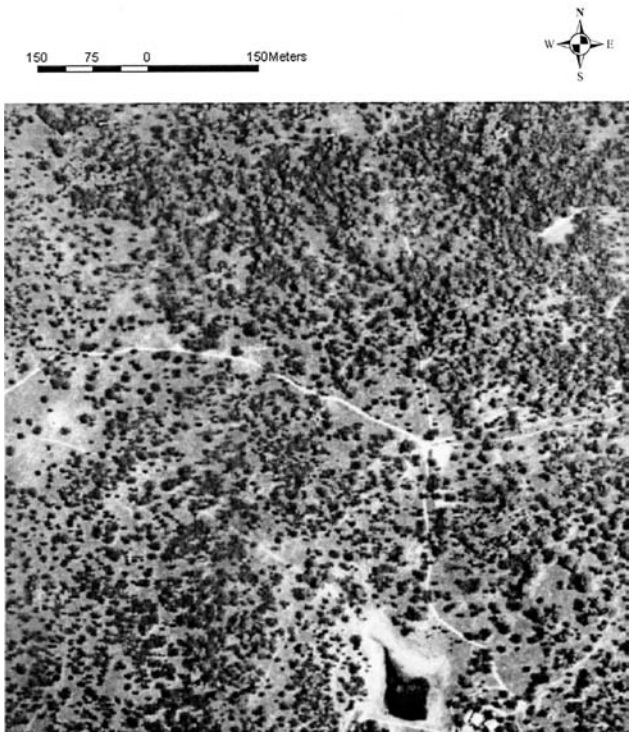

Figure 1. A CASI image covering the study area.

Methods

Study Area and Lidar Data

The study site is an open oak savanna woodland, located near Ione, California (latitude: 38.26° N, longitude: 120.57° W) (Figure 1). The site is on a private ranch and is part of the AmeriFlux network of eddy covariance field sites (Baldocchi *et al.*, 2004). The landscape is characterized by flat terrain (with a maximum slope of less than 15 percent) with a scattered, clumped distribution of blue oaks (*Quercus douglasii H.&A.*) and a minority of grey pines over a continuous layer of Mediterranean annual grasses. On 24 August 2003, laser altimetry data were acquired with Optech ALTM 2025, which recorded both first and last returns for each laser pulse. The scanning pattern was z-shape. The claimed vertical accuracy from the data provider is 18 cm with 95 percent confidence and the horizontal accuracy is 1/3000 of the flying height. The swath is approximately 300 m and the flying altitude is approximately 500 m. The footprint size is about 18 cm. The average posting density is 9.5 points per square meter, resulting in an average spot spacing of about 32 cm. To obtain such a high pulse density, the site was flown twice. The data covering 800 m by 800 m around the eddy covariance tower was used in this study to isolate individual trees.

Digital Elevation Model

The tree isolation from lidar data is typically based on a canopy height model (CHM), which is the difference between canopy surface height and a digital elevation model (DEM) of the earth surface. The research on generating a DEM from laser altimetry data, also called *filtering*, is still being developed. Typically, the laser pulses are classified iteratively into terrain and non-terrain returns, and the extracted terrain pulses are used to generate a DEM by interpolation (Hyyppä *et al.*, 2001; Persson *et al.*, 2002; Brandtberg *et al.*, 2003). In this study, the basic procedure of generating a DEM is as follows:

First, a grid with cell size of 1 m by 1 m was created. Each cell recorded the lowest last return of all pulses falling in the cell; this grid is denoted as $g_{\min}$. If some cells have no pulses within them, they were filled with the nearest cell value; this filled grid is denoted as $g_{f\min}$. Then, a surface approximating the terrain, denoted as $g_{o(f\min)}$, was created by morphologically opening the filled grid $g_{f\min}$. An initial set of terrain pulses were identified by calculating the difference between $g_{\min}$ and $g_{f\min}$. The cells with absolute value of difference less than 0.5 m were treated as cells where terrain pulses are located. The triplex $\{X_i, Y_i, g_{\min,i}\}$ from these cells were used to create a DEM by kriging. A new set of terrain pulses were obtained by comparing the elevation of last return of each pulse with its DEM value. If their absolute value of difference was less than 0.5 m, it was classified as a terrain pulse. The details on the algorithm are presented in another companion paper (Chen *et al.*, 2007). Figure 2 shows the DEM.

To assess the accuracy of filtering, three plots, each with an area of 100 m by 100 m, were randomly located and the pulses were manually classified into terrain and vegetation returns, and this layer acted as subsequent ground truth. The accuracy of filtering was evaluated by calculating the type I, type II and total error (Sithole and Vosselman, 2003). Type I error is the percentage of terrain returns misclassified as vegetation returns. Type II error is the percentage of vegetation returns misclassified as terrain returns. Total error is the error weighted with the portion of each category of reference returns. The accuracy

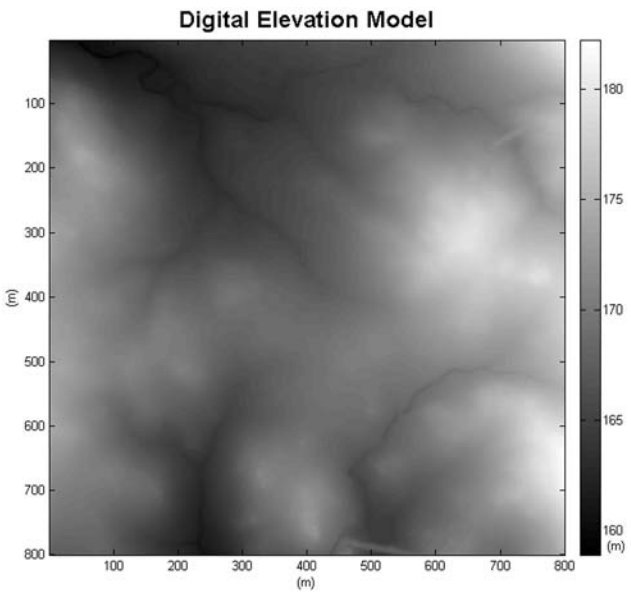

Figure 2. The DEM generated from lidar data.

TABLE 1. FILTERING ACCURACY ASSESSMENT TABLE FOR ALL PLOTS

All Plots		Filtered: Terrain	Filtered: Vegetation	Total	Error (%)
Reference	Terrain	218189	2305	220494	1.04
	Vegetation	1650	92479	94129	1.75
	Total	18647	19363	314623	1.26

is summarized in Table 1. The high accuracy of filtering is partially due to the flat terrain over the study area.

Canopy Height Model

After the DEM has been created, the relative canopy height of laser pulses can be calculated and interpolated into a CHM. Previous research used kriging (Popescu and Wynne, 2004), active contour algorithm (Persson *et al.*, 2002), or VDEMINT program in PCI EASI (Leckie *et al.*, 2003) to create a CHM or digital surface model (DSM). In Popescu and Wynne (2004), at first a grid was created, each cell of which recorded the elevation of the highest first-return of laser pulses within it; then, the elevations within these cells were interpolated into a CHM by kriging. This method is used in this study. The cell size of the grid is an important parameter in constructing a CHM. A large cell size will reduce the variations of canopy height and make the "peaks" and "valleys" difficult to detect in the interpolated CHM. Nevertheless, a very small cell size could dramatically increase the data storage. If first-return density λ (returns/m^2) does not change over the study area, the average distance between pulses is:

$$d = \sqrt{\frac{1}{\lambda}} \tag{1}$$

and cell size can be set to d. In practice, pulse density varies because there are side overlaps between swaths and pulse density is higher along the edges of a swath for this dataset. Therefore, a small cell size should be used when there are large pulse densities locally. The variations of λ were investigated by overlaying a grid of 1 m by 1 m cells over the first-returns. Results showed that λ varied from 0 to 115 returns per m^2. A large λ was chosen by calculating the p^{th} quantile of λ. In this study, p was set to be 0.99 and its corresponding λ value was 44. With Equation 1, the cell size was set to be 0.2 m.

Variable Window Sizes in Treetops Detection

Treetops can be detected by finding the local maxima (Hyyppä *et al.*, 2001; Persson *et al.*, 2002) or local maxima within fixed or variable window sizes in a CHM (Dralle and Rudemo, 1996; Wulder *et al.*, 2000). The main problem encountered when using local maxima to detect treetops is large commission errors, that is, non-treetop local maxima are incorrectly classified as treetops. Wulder *et al.* (2000) detected treetops from high spatial resolution optical imagery by searching local maxima within variable window sizes. The window sizes were adaptively calculated based on the semivariance range or local breaks in slope. Popescu and Wynne (2004) derived variable window sizes by assuming a relationship between tree height and crown size and used them to detect treetops from lidar data. The Popescu and Wynne (2004) method was tested in this dataset.

To obtain a relationship between tree height and crown size, tree height and crown size were measured manually from the CHM. Tree height is the maximum height within a manually determined crown. Crown size is the average crown diameter along two perpendicular directions. The trees were sampled systematically over the whole study area with horizontal and vertical intervals of 53 m. If there were no trees in the sampling locations, the nearest tree was selected. The final sample size was 196 trees.

There are several reasons for measuring tree height and crown sizes from the CHM rather than in the field. First, due to high pulse density of this lidar dataset, it is easy to identify individual trees from the CHM manually. Second, sampling in a CHM can greatly reduce the workload and is not limited by factors such as accessibility in the field. To evaluate the accuracy, another 26 trees were randomly chosen and their tree height and crown size of measured from both CHM and the field. In the field, the height of each tree was measured with a hypsometer for eight times and the measurements were averaged. Crown size was measured along two perpendicular directions, and the average value was used. The mean absolute differences of tree height and crown size between CHM and field measurements were 0.37 m and 0.58 m, respectively. This indicates that the accuracy is acceptable when sampling trees from CHM.

It was found that crown size has larger variability when a tree is higher (Figure 3), which will violate the assumption of homoscadasticity if a linear model is fitted. To avoid this issue, a nonlinear power model was fitted:

$$\text{Crown size} = 1.7425 \times (\text{Tree height})^{0.5566}. \tag{2}$$

Variable Window Size from Prediction Interval

Using Equation (2), the commission errors can be reduced, since it will search local maxima within larger window sizes for higher trees. However, this will also lead to large omission errors. Statistically, a half number of the trees at a certain height have smaller crown sizes than the fitted value at this height (Figure 3). The treetops of these trees will possibly be missed if the window size is equal to the fitted value. In this study, the window sizes were determined by another curve which is the 1-α lower limit of one-sided prediction interval of the regression model (Figure 3). Consider a regression model $Y_x = \beta^T x + \varepsilon_i$. The curve is determined by:

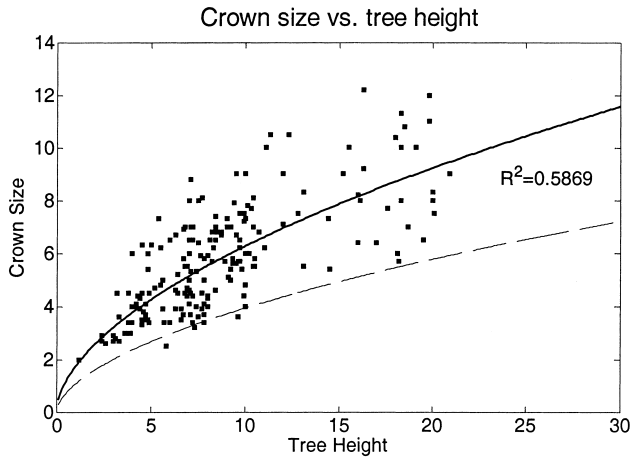

Figure 3. The relationship between crown size and tree height. The solid line is the regressive curve and the dashed line is the lower limit of the prediction intervals.

$$\tilde{Y}_x = \hat{Y} - t(1\text{-}\alpha;n\text{-}2)\sqrt{s^2 + xSx'} \quad (3)$$

where $\tilde{Y}_x$ is the lower prediction limit at a given tree height x, s^2 is the mean squared error, t is the inverse of Student's t cumulative distribution function, S is the covariance matrix of the coefficient estimates, $(X^TX)^{-1}s^2$, and $\hat{Y}$ is the fitted value at x. When α is 0.5, the lower limit $\tilde{Y}_x$ is exactly located at the fitted regression curve. When using this curve to determine window sizes for detecting treetops, the omission errors can be reduced by using a small α. However, a smaller α will lead to larger commission errors (see Figures 4b and 4c). Only if the window size is smaller than the crown size of a tree, there is a risk of including irrelevant local maxima as treetops.

Canopy Maxima Model

The previous analysis demonstrated that commission and omission errors of treetop detection cannot be decreased simultaneously by adjusting α when a canopy height model was used. This problem can be greatly alleviated when detecting treetops from a canopy maxima model (CMM), which is a regular grid with each cell recording the maximum laser height within its neighborhood. Compared with a CHM, many irrelevant local maxima can be removed in the CMM (Figure 4d). As detecting treetop markers, variable window sizes are used to creating a CMM. To prevent the "valleys" among crowns from being filled, the window size need to be smaller than the crown size of the smallest tree at a given height. This can be approximated statistically by obtaining the lower limit of one-sided prediction interval with a very small α in Equation 3. Previous researchers have reported that the tree density for blue oaks on gentle slopes has a maximum tree density of about 200 trees/ha (Kiang, 2002). Corresponding to such a number there is a maximum of about 12,800 trees for the study area of 800 m by 800 m. Based on this, α is set to be 0.0001. The tree height from the CHM was used to determine the window sizes with Equation 3.

Gaussian Filtering

In the CMM, not all of the non-treetop local maxima could be removed since the neighborhood window size used for creating the CMM is usually smaller than the crown size, especially for trees which have large crowns at a certain

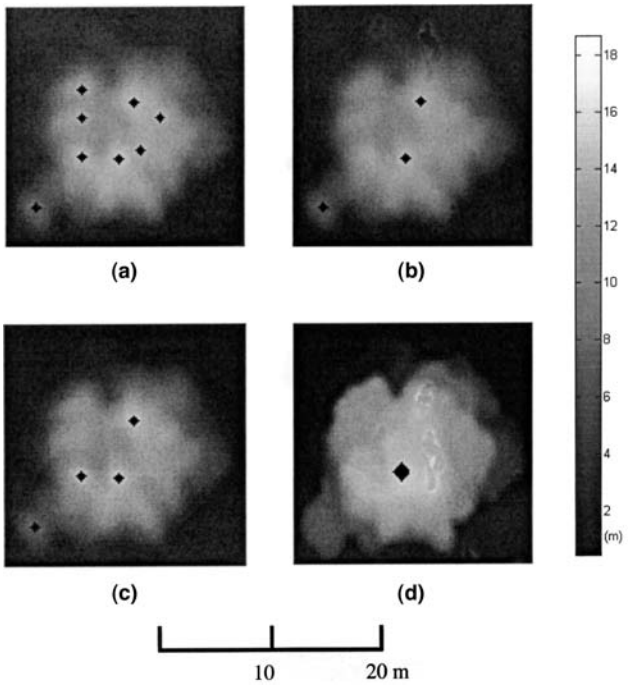

Figure 4. Treetops detected using different methods and parameters. (a) Treetops detected from a CHM by searching local regional maxima, (b) treetops detected from a CHM using variable window size when α = 0.5, (c) treetops detected from a CHM using variable window sizes when α = 0.1, and (d) treetops detected from a CMM using variable window size when α = 0.1.

height. Gaussian filtering is a typical procedure for suppressing irrelevant local maxima in treetop detection (Dralle and Rudemo, 1996; Hyyppä *et al.*, 2001; Persson *et al.*, 2002; Pouliot *et al.*, 2002; Schardt *et al.*, 2002; Wang *et al.*, 2004). Dralle and Rudemo (1996) found that the standard deviation σ of a Gaussian filter is not very important. This conclusion was confirmed in this study and the value of σ was set to be 2. However, the filter size has a significant impact on the smoothed CMM. This study used the criteria that the filter size should not be larger than the crown size of the smallest (in terms of crown) tree over the study area. The determination of the smallest crown size was based on the crown sizes of the sampled trees from the CHM. The smallest crown size can be approximated from the sample by calculating the lower limit of the one-sided prediction intervals for k future observations at confidence level (1-α) (Hahn and Meeker, 1991):

$$\text{Lower Limit} = \overline{X} - t_{1-\frac{\alpha}{k}}(n-1)s\sqrt{1+\frac{1}{n}}, \quad (4)$$

where $\overline{X}$, s, n are the mean, standard deviation, and size of the sample of crown size, respectively (Table 2); α was set to be 0.05. Based on the previous analysis, k was set to be 12,800.

When checking the crown size distribution of the sample, it was found that the distribution was skewed to the right. A Jarque-Bera test for the goodness-of-fit of normal distribution indicated that the p-value was 0.0016, which was significantly different from a normal distribution at 5 percent level. When transformed into logarithm scale (with natural base e), the p-value was 0.2224. Therefore, Equation 4

TABLE 2. DESCRIPTIVE STATISTICS OF SAMPLED TREES (N = 196)

Variables	Min(m)	Max(m)	Mean(m)	Std.(m)
Tree height	2.0	12.2	5.8	2.1
Crown size	1.2	20.9	8.8	4.4

was used to get the lower limit of the one-sided prediction interval of crown sizes at the logarithmic scale. After transformed back to the original scale, a value of 1.0 m was obtained for the minimal crown size, which was used as the Gaussian filter size.

In a smoothed CMM, the spurious local maxima other than treetops were greatly reduced (see Figures 4c and 4d) and the change of α in Equation 4 would affect mostly the omission errors not the commission errors. Applying such a "divide-and-conquer" strategy, both the omission and commission errors for treetop detection can be reduced. After treetops had been detected, they were used for segmenting individual crowns.

Segmentation with CMM

The process of watershed segmentation can be illustrated in terms of flooding simulations (Soille, 2003). Figure 5a shows a CMM. To simulate the process of flooding, we first calculated the complement of the CMM (Figure 5b), which resembles two catchment basins. Assume that each basin has a hole punched at its minimum. Then, when immersing it gradually into water, the catchment basins will be flooded. This algorithm can be thought to automatically build dams along the divide line to prevent water in two neighboring catchment basins from merging (Figure 5c). The constructed dams are called watershed lines and will be used to partition trees.

In marker-controlled watershed segmentation, the complement of the CMM is filtered by *minima imposition* before computing its watersheds so that all non-treetop minima have been removed. Suppose there is an image f, which is the complement of the CMM in this case, and a marker image f_m has been specified at each pixel p:

$$f_m(p) = \begin{cases} 0, \text{ if } p \text{ belong to a marker,} \\ t_{\max} + 1, \quad \text{otherwise.} \end{cases} \tag{5}$$

where $t_{\max}$ is the maximum value of the input image f. Minima imposition is to first calculate a pixel-wise minimum between $f + 1$ and the marker image f_m, denoted as $(f + 1) \wedge f_m$, and then perform a morphological reconstruction by erosion of $(f + 1) \wedge f_m$ from the marker image f_m:

$$f_{mp} = R^{\varepsilon}_{(f+1)\wedge f_m}(f_m), \tag{6}$$

where f_{mp} is the image after minima imposition, $R^{\varepsilon}_{(f+1)\wedge f_m}(f_m)$ is defined as the geodesic erosion of $(f + 1) \wedge f_m$ with respect to f_m iterated until stability is reached (Soille, 2003). The geodesic erosion of $(f + 1) \wedge f_m$ with respect to f_m is to perform morphological erosion for f_m, but the value of $(f + 1) \wedge f_m$ is used only if the value after erosion is smaller than $(f + 1) \wedge f_m$. Minima imposition can reconstruct the complement of CMM so that there are only minima corresponding to marked treetops. This illustration highlights the importance of finding a correct treetop marker function when applying marker-controlled watershed segmentation method.

Segmentation with Distance-Transformed Image

Deciduous trees, such as oak, have a relatively flat canopy surface making treetops difficult to detect from the CMM or CHM (Figure 6a). Since treetops are typically located around the center of crowns, this fact can be exploited to further detect treetops. To implement that, at first, a binary image was created, where the canopy had values of ones while watershed lines and the background had values of zeros (Figure 6b). Then, a distance transform was performed on the binary image to calculate the distance from each non-zero pixel to its nearest zero pixel (Figure 6c). In the distance-transformed image, the center of a crown had large values. Like the CMM, the complement of this distance-transformed image, denoted as $DIST_c$, can be used for segmentation. Treetops were detected from $DIST_c$ using h-minima transformation which suppressed all minima shallower than h. The h-minima transformation of the $DIST_c$ is to perform the reconstruction by erosion of $DIST_c$ from $DIST_c + h$.

$$DIST_{c,h\min} = R^{\varepsilon}_{DIST_c}(DIST_c + h) \tag{7}$$

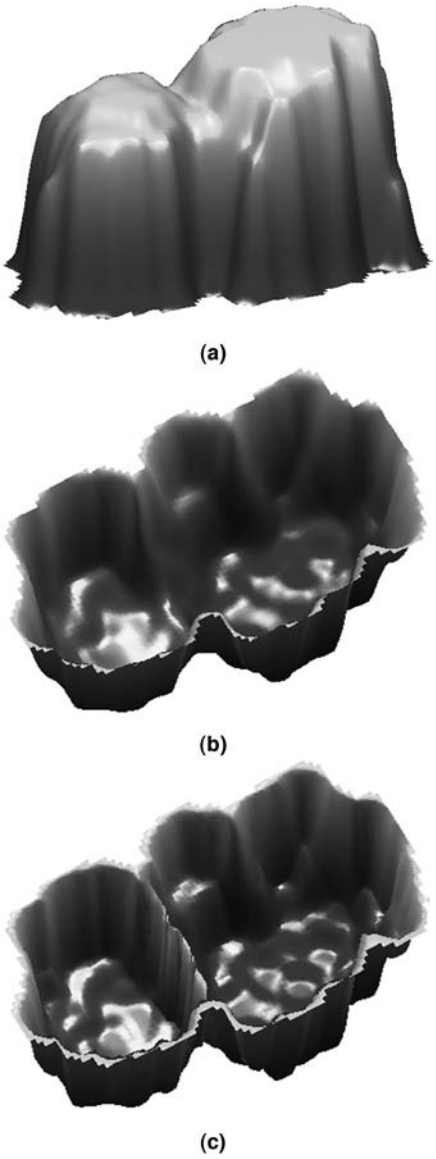

Figure 5. An illustration of watershed segmentation Algorithm. (a) A CMM, (b) the complement of the CMM, and (c) dams built at the divide line.

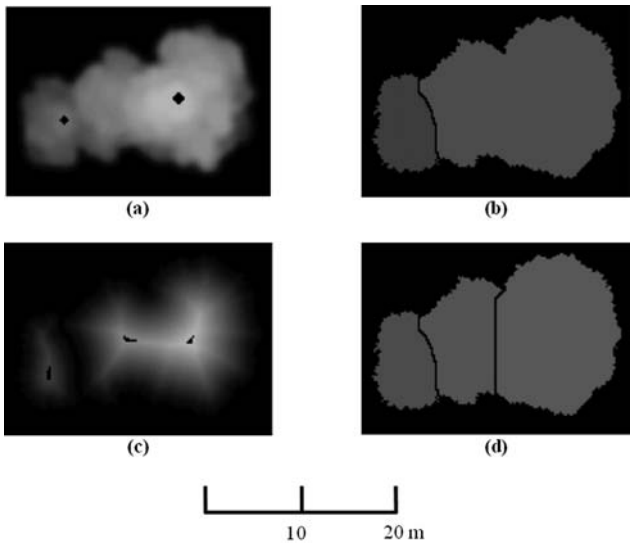

Figure 6. Distance-transformed image for treetops detection. (a) Treetops found in CMM, (b) segmentation results using treetops in CMM, (c) distance-transformed image and treetops detected using h-minima transform, and (d) segmentation results based on distance-transformed image.

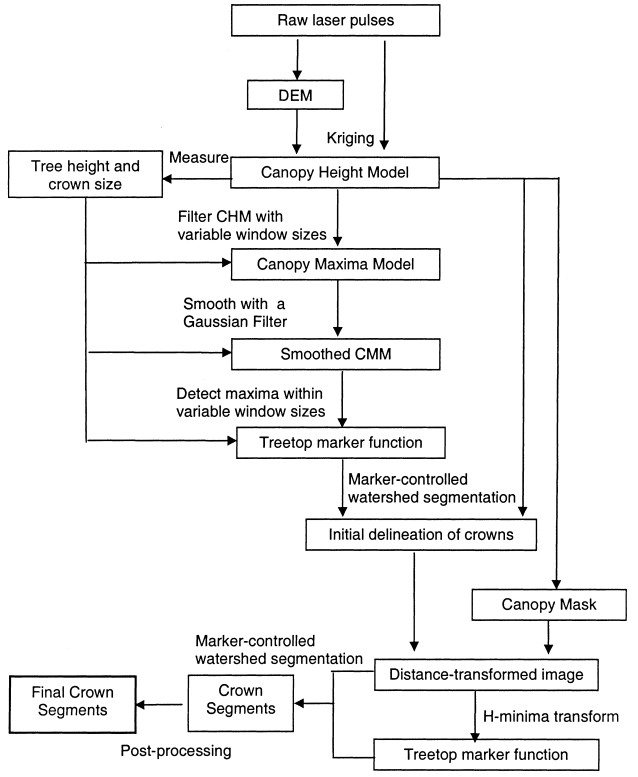

Figure 7. Flow chart of the method for tree isolation.

where $DIST_{c,h\min}$ is the h-minima transformation of $DIST_c$. The regional minima of $DIST_{c,h\min}$ was marked as treetops. With these treetop markers and the segmentation function $DIST_c$, marker-controlled watershed segmentation was used for delineating tree crown segments (Figure 6d). Note that the threshold h directly affects the performance of detecting treetops. An optimal value of h was obtained from the training data.

Because there are some dead trunks and some instruments for ecological studies in the sites, the segments were post-processed by removing all segments which are shorter than 2 m. Also all segments adjoining the boundary of the study site were removed. The whole procedure for isolating individual trees is illustrated in Figure 7.

Results and Discussions

Accuracy Assessment

To evaluate accuracy, a ground truth crown map for two transects (Figure 8), each with an area of 100 m by 300 m, was acquired by manually delineating the crowns boundaries on the prints of the CHM in the field. Airphotos were used in the field to aid the delineation of tree crowns. After the crown boundaries had been outlined in the field, they were further verified and refined by examining the laser point cloud with a 3D visualization software (ArcGIS® 3D Analyst, ESRI™) in the laboratory. There are a total of 772 trees in the two transects. The absolute accuracy for tree isolation (AATI) was used for evaluating delineation accuracy:

$$\mathrm{AATI} = \frac{N_{1,1}}{N_r} \tag{8}$$

where $N_{1,1}$ is the number of crowns which has one-to-one relationship with the ground truth crown polygon, N_r is the number of crowns in the field, and N_s is the total number of automatically delineated segments. One-to-one relationship means that the overlaying area S_o between a ground truth crown polygon and one segment overlaying with it is within the range of $S_r \pm 10\% * S_r$, where S_r is the area of the reference crown polygon.

There are two free parameters in the tree isolation method: α in Equation 4 and h in Equation 7. The tree isolation accuracy was assessed by the five-fold, cross-validation method, which divided the ground truth data into five folds randomly. Each time four folds were used for training and the parameters that achieved the highest AATI for the training data were used to evaluate the accuracy of the fold left out. This process was repeated for five times and the accuracies for five folds were averaged. When parameters were tuned, the domains of α and h were limited to be {0.01, 0.1, 0.2, 0.3, 0.4, 0.5} and {0.1, 0.2, 0.3, 0.4, 0.5, 0.6, 0.7}, respectively. It was found that when any four folds were used for training, the highest AATI was obtained when the highest AATI was obtained when α was 0.01 and h was 0.5 m. The AATI for different folds varied from 61.3 percent to 68.2 percent. The average cross-validation accuracy was 64.1 percent. With these parameters values, there were a total of 9,386 segments delineated (Figure 8).

Because different studies use different accuracy assessment methods, it is difficult to compare our accuracy with those from other studies. Persson *et al.* (2002) delineated crown segments of conifers such as Norway spruce, Scot pines, and Birch in southern Sweden. They linked the segments with field trees by searching all segments within two pixels (two-thirds of a meter) around a field tree. In total, 71 percent of trees were correctly detected. Brandtberg *et al.* (2003) adopted the fuzzy concept to quantify the accuracy of the segmentation results and designed an index A, the value of which is 1 if the segment polygon overlaid perfectly with the delineated polygon in the field. Finally, their A values varied from 0.21 to 0.35 for six one-hectare

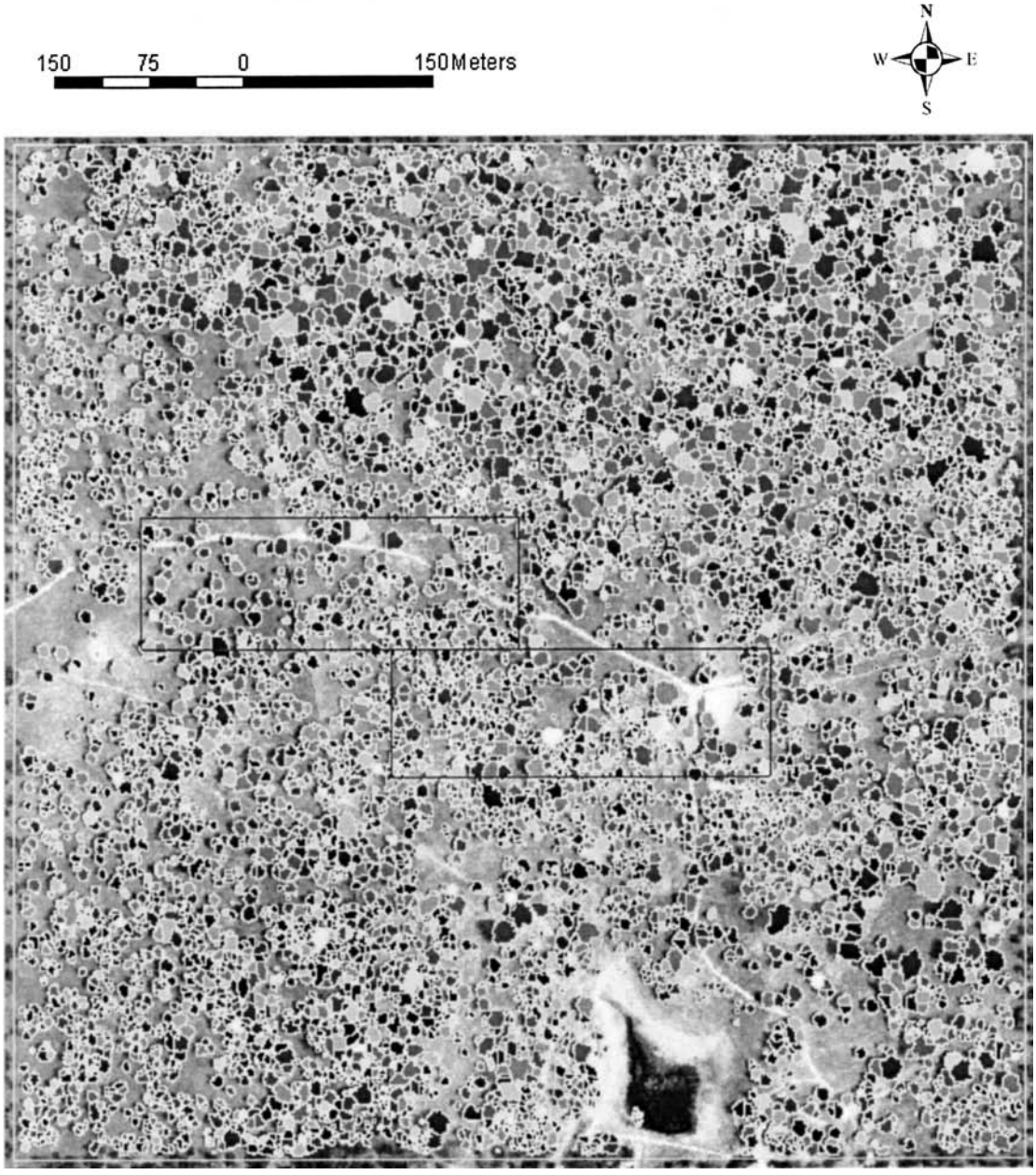

Figure 8. Crown delineation map (α = 0.01 and h = 0.5m). The two rectangles show the locations of transects for accuracy assessment.

plots in a deciduous forest with species including oaks, maple and poplar. Leckie *et al.* (2003) treated it as a "perfect" match when there is a one-to-one correspondence between ground reference polygons and delineated segments and their overlaps are greater than 50 percent. They obtained a 59 percent "perfect" match for a conifer forest. When compared with these studies, the criteria for accuracy assessment used in this study are much stricter. Therefore, the accuracy obtained with our method is encouraging.

Effects of α and h

To examine the effects of α and h, the AATIs for all combinations of these two parameters were calculated for all trees in the ground truth transects (Table 3). When investigating the effects of the threshold h on tree isolation accuracy, there was a consistent pattern showing that h = 0.5 m is the best value for this dataset (Figure 9a). When h is very small, spurious local minima could be counted as treetops and tree crowns will be over-segmented. When h is very large, treetops will be missed, leading to the under-segmentation issues. Therefore, when h lies between these two extrema, the highest accuracy can be obtained. For α, it seems that the tree isolation accuracy increases when decreasing α. One of the possible reasons is that when using smoothed CMM to detect treetops, the commission errors have been greatly reduced. As a result, decreasing α will reduce the omission errors while having little effects on the commission errors (Figure 9b).

TABLE 3. TREE ISOLATION ACCURACY

AATI	h = 0.1	h = 0.2	h = 0.3	h = 0.4	h = 0.5	h = 0.6	h = 0.7
α = 0.01	59.2%	60.8%	62.0%	62.8%	64.1%	63.3%	62.3%
α = 0.1	58.4%	59.2%	60.5%	61.9%	62.8%	61.7%	60.1%
α = 0.2	57.9%	58.2%	58.8%	60.4%	62.6%	61.3%	59.8%
α = 0.3	57.3%	57.1%	57.6%	58.4%	59.7%	58.4%	56.9%
α = 0.4	57.0%	56.9%	57.5%	58.2%	59.2%	58.2%	56.9%
α = 0.5	56.7%	56.6%	57.3%	57.8%	58.8%	57.5%	56.1%

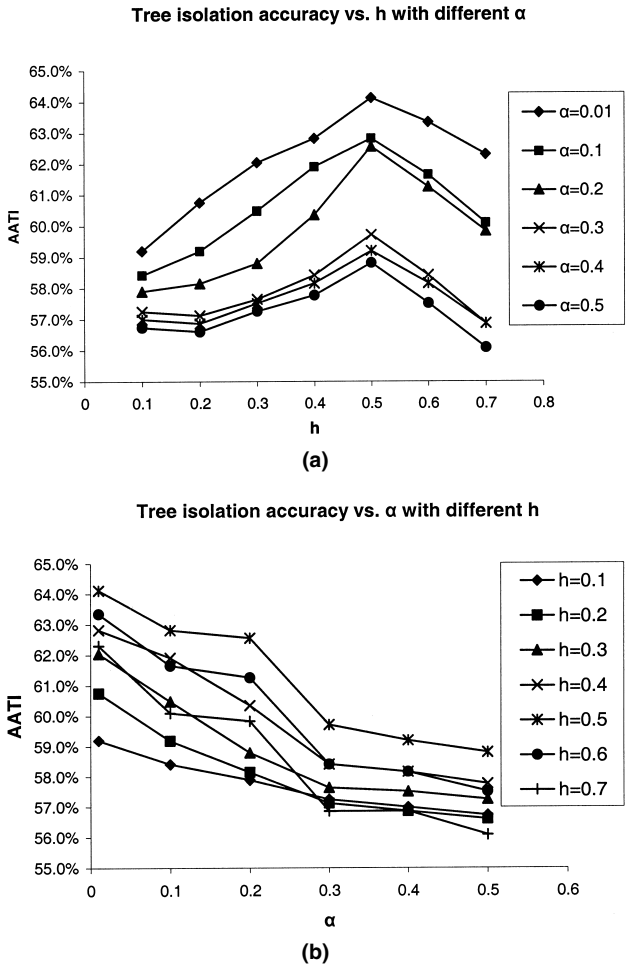

Figure 9. The effects of parameters on tree isolation.

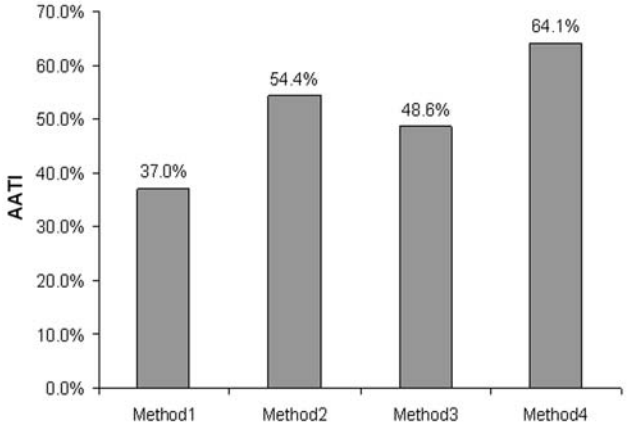

Figure 10. Comparison of tree isolation accuracy from different treetop detection methods. Method 1: detect treetops from CHM and window sizes are based on the fitted regression curve; Method 2: detect treetops from CMM and window sizes are based on the lower-limit of the prediction interval of the regression curve; Method 3: treetops are local maxima within CHM; and Method 4: detect treetops from distance-transformed image in addition to Method 3.

Comparison of Different Treetop-detection Methods

In addition to the above method, three other methods of treetop detection were applied into marker-controlled watershed segmentation for tree isolation: (a) the first method was based on Popescu and Wynne (2004), which detected treetops by searching local maxima within variable window sizes in the CHM. The window sizes were determined by the fitted regression curve, (b) in the second method, treetops were detected from the CMM and variable window sizes were determined by the lower-limit of the prediction interval of the regression curve, but the distance-transformed image was not used for detecting treetops, and (c) in the third method, treetops were detected by finding local maxima in the CHM. For all of these three methods, the segmentation function is the CHM.

The AATIs for these three methods were 37.0 percent, 54.4 percent, and 48.6 percent, respectively (Figure 10). The method based on Popescu and Wynne (2004) had the lowest accuracy. This is not surprising since previous analysis shows that potentially about a half number of trees would be missed if window sizes are determined by the fitted regression curve. In the second method, the accuracy was much higher than that in the first method when treetops were detected from the CMM and the window sizes were determined by the lower-limit of the prediction interval. Compared with the second method, the method which additionally detected treetops from distance-transformed image can increase the accuracy by about 10 percent. The accuracy from the third method is also higher than the Popescu and Wynne (2004) method. This is because the omission errors in this method are low.

Error Analysis

The omission and commission errors will lead to under- or over-segmentation of tree crowns. When the branches of neighboring trees are intertwined or trees with different heights are growing closely, it is usually difficult to separate them. The over-segmentation problem mostly occurred for very old oak trees. These old and large oak trees usually grow in open space. With little competition of light and nutrient with surrounding trees, their branches can reach far in various directions and grow into irregular shape. When each large branch looks like a tree, the over-segmentation

problem happens. When the "valleys" among trees were not discernable in CMM or distance-transformed image, the crown boundaries were wrongly delineated.

Conclusion

In this study, previous methods of detecting treetops by searching local maxima within variable window sizes were revisited and it was found that using fitted regression curve to determine window sizes could lead to large omission errors. The proposed method intended to reduce the omission and commission errors in three means: (a) creating a CMM to reduce the spurious local maxima, (b) detecting treetops from the CMM using variable window sizes which were based on the lower limit of the prediction intervals, and (c) detecting treetops using distance-transform, which was based on the fact that treetops are located around the center of each crowns. The first means was to reduce commission errors and the rest two were to reduce omission errors. It was found that this "divide-and-conquer" method can achieve much higher accuracy than traditional methods. Also, applying distance-transform image to detect treetops can significantly increase the tree isolation accuracy. However, compared with previous methods, this method requires field data to train two additional parameters α and h. More research is needed to test this method over other forest types and examine the effects of α and h. Overall, the accuracy of this method is encouraging, especially considering the strict criteria used in accuracy assessment. The results showed that marker-controlled watershed segmentation can be used for isolating individual trees for deciduous tree species. The tree isolation results can be further used to extract other forest parameters such as tree height, crown size, biomass, and LAI. With individual tree information extracted from remotely sensed data, biogeochemistry models can be parameterized to scale up from individual trees to landscapes for better understanding of various ecological processes.

Acknowledgments

We appreciate the constructive comments from the three anonymous reviewers. Qi Chen is thankful for the support from the NASA Earth System Science Graduate Student Fellowship and the Berkeley Atmospheric Sciences Center (B.A.S.C) Fellowship.

References

Baldocchi, D.D., L. Xu, and N. Kiang, 2004. How plant functional-type, weather, seasonal drought, and soil physical properties alter water and energy fluxes of an oak-grass savanna and an annual grassland, *Agricultural and Forest Meteorology*, 123:13–39.

Beucher, S., and C. Lantuejoul, 1979. Use of watersheds in contour detection, *International Workshop on Image Processing, Real-time Edge and Motion Detection/Estimation*, Rennes, France.

Brandtberg, T., and F. Walter, 1998. Automated delineation of individual tree crowns in high spatial resolution aerial images by multiple-scale analysis, *Machine Vision and Applications*, 11:64–73.

Brandtberg, T., T.A. Warner, R.E. Landenberger, and J.B. McGraw, 2003. Detection and analysis of individual leaf-off tree crowns in small footprint, high sampling density lidar data from eastern deciduous forest in North America, *Remote Sensing of Environment*, 85:290–303.

Chen, Q., P. Gong, and D.D. Baldocchi., 2007. Filtering airborne laser scanning data with morphological methods, *Photogrammetric Engineering & Remote Sensing*, In press.

Clark, D.B., C.S. Castro, L.D.A. Alvarado, and J.M. Read, 2004a. Quantifying mortality of tropical rain forest trees using high-spatial-resolution satellite data, *Ecological Letters*, 7:52–59.

Clark, D.B., J.M. Read, M.L. Clark, A.M. Cruz, M.F. Dotti, and D.A. Clark, 2004b. Application of 1-m and 4-m resolution satellite data to ecological studies of tropical rain forests, *Ecological Applications*, 14:61–74.

Dralle, K., and M. Rudemo, 1996. Stem number estimation by kernel smoothing of aerial photos, *Canadian Journal of Forest Research*, 26:1228–1236.

Gong, P., G.S. Biging, S.M. Lee, X. Mei, Y. Sheng, R. Pu, B. Xu, K. Schwarz, and M. Mostafa, 1999. Photo ecometrics for forest inventory, *Geographic Information Science*, 5:9–14.

Gong, P., Y. Sheng, and G.S. Biging, 2002. 3D Model-based Tree measurement from high-resolution aerial imagery, *Photogrammetric Engineering & Remote Sensing*, 68:203–1212.

Gougeon, F.A., 1995. A crown-following approach to the automatic delineation of individual tree crowns in high spatial resolution aerial images, *Canadian Journal of Remote Sensing*, 21:274–284.

Gougeon, F.A., and D.G. Leckie, 1999. Forest regeneration: Individual tree crown detection techniques for density and stocking assessment, *Proceedings of the International Forum on Automated Interpretation of High Spatial Resolution Digital Imagery for Forestry*, 10–12 February 1998, Victoria, B.C., Pacific Forestry Center, Canadian Forest Service, Natural Resources Canada, pp. 11–23.

Hahn, G.H., and W.Q. Meeker, 1991. *Statistical Intervals: A Guide for Practitioners*, John Wiley & Sons, Inc., New York.

Hyyppä, J., O. Kelle, M. Lehikoinen, and M. Inkinen, 2001. A segmentation-based method to retrieve stem volume estimates from 3-D tree height models produced by laser scanners, *IEEE Transactions on Geoscience and Remote Sensing*, 39:969–975.

Kelly, M., D. Shaari, Q.H. Guo, and D.S. Liu, 2004. A comparison of standard and hybrid classifier methods for mapping hardwood mortality in areas affected by "sudden oak death," *Photogrammetric Engineering & Remote Sensing*, 70:1229–1239.

Kiang, N.Y., 2002. *Savannas and Seasonal Drought: The Landscape-leaf Connection Through Optimal Stomatal Control*, Ph.D. dissertation, Department of Environmental Science, Policy, and Management, University of California at Berkeley, Berkeley, California, 303 p.

Larsen, M., and M. Rudemo, 1998. Optimizing templates for finding trees in aerial photographs, *Pattern Recognition Letters*, 19(12): 1153–1162.

Leckie, D.G., X. Yuan, D.P. Ostaff, H. Piene, and D.A. Maclean, 1992. Analysis of high spatial resolution multispectral MEIS imagery for spruce budworm damage assessment on a single tree basis, *Remote Sensing of Environment*, 40:125–136.

Leckie D., F. Gougeon, D. Hill, R. Quinn, L. Armstrong, and R. Shreenan, 2003. Combined high-density lidar and multispectral imagery for individual tree crown analysis, *Canadian Journal of Remote Sensing*, 29(5):1–17.

Levesque, J., and D.J. King, 1999. Airborne digital camera image semivariance for evaluation of forest structural damage at an acid mine site, *Remote Sensing of Environment*, 68:112–124.

Meyer, F., and S. Beucher, 1990. Morphological segmentation, *Journal of Visual Communication and Image Representation*, 1:21–46.

Persson, Å., J. Holmgren, and U. Söderman, 2002. Detecting and measuring individual trees using an airborne laser scanner, *Photogrammetric Engineering & Remote Sensing*, 68:925–932.

Pollock, R., 1996. *The Automatic Recognition of Individual Trees in Aerial Images of Forests Based on a Synthetic Tree Crown Model*, Ph.D. dissertation, Department of Computer Science, University of British Columbia, Vancouver, B.C.

Popescu, S.C., R.H. Wynne, and R.F. Nelson, 2003. Measuring individual tree crown diameter with lidar and assessing its influence on estimating forest volume and biomass, *Canadian Journal of Remote Sensing*, 29:564–577.

Popescu, S.C., and R.H. Wynne, 2004. Seeing the trees in the forest: Using lidar and multispectral data fusion with local filtering and variable window size for estimating tree height, *Photogrammetric Engineering & Remote Sensing*, 70:589–604.

Pouliot, D.A., D.J. King, F.W. Bell, and D.G. Pitt, 2002. Automated tree crown detection and delineation in high-resolution digital camera imagery of coniferous forest regeneration, *Remote Sensing of Environment*, 82:322–334.

Schardt, M., M. Ziegler, A. Wimmer, R. Wack, and J. Hyyppae, 2002. Assessment of Forest Parameters by Means of Laser Scanning, *International Archives of Photogrammetry and Remote Sensing*, XXXIV part 3A. pp. 302–309.

Sithole, G., and G. Vosselman, 2003. Comparison of filtering algorithms, *Proceedings of the ISPRS Working Group III/3 Workshop: 3-D Reconstruction from Airborne Laserscanner and InSAR data*, October, Dresden, Germany, URL:http://www.isprs.org/commission3/wg3/workshop_laserscanning/, (last date accessed: 09 May 2006)

Soille, P., 2003. *Morphological Image Analysis: Principles and Applications*, 2nd edition, Springer-Verlag, Berlin, Germany, 391 p.

Wang, L., P. Gong, and G.S. Biging, 2004. Individual tree-crown delineation and treetop detection in high-spatial-resolution aerial imagery, *Photogrammetric Engineering & Remote Sensing*, 70:351–358.

Wulder, M., K.O. Niemann, and D. Goodenough, 2000. Local maximum filtering for the extraction of tree locations and basal area from high spatial resolution imagery, *Remote Sensing of Environment*, 73:103–114.

(Received 05 April 2005; accepted 13 July 2005; revised 21 July 2005)